2003

Ozone, aerosol, potential vorticity, and trace gas trends observed at high-latitudes over North America from February to May 2000

Edward V. Browell
NASA

Jonathan Hair
NASA

Carolyn Butler
NASA

William B. Grant
NASA

Russell J. DeYoung
NASA

See next page for additional authors

Recommended Citation

Browell, E. V., et al. (2003), Ozone, aerosol, potential vorticity, and trace gas trends observed at high-latitudes over North America from February to May 2000, J. Geophys. Res., 108, 8369, doi:10.1029/2001JD001390, D4.

Authors

Edward V. Browell, Jonathan Hair, Carolyn Butler, William B. Grant, Russell J. DeYoung, Marta Fenn, Vincent G. Brackett, Marian B. Clayton, Lorraine A. Brasseur, David B. Harper, Brian Ridley, Andrzej Klonecki, Peter Hess, L K. Emmons, Xuexi Tie, Elliot Atlas, C A. Cantrell, Anthony Wimmers, D R. Blake, Michael T. Coffey, James W. Hannigan, Jack E. Dibb, R. Talbot, F Flocke, Andrew Weinheimer, A Fried, B Wert, J Snow, and Barry Lefer

Ozone, aerosol, potential vorticity, and trace gas trends observed at high-latitudes over North America from February to May 2000

Edward V. Browell,[1] Johnathan W. Hair,[1] Carolyn F. Butler,[2] William B. Grant,[1] Russell J. DeYoung,[1] Marta A. Fenn,[2] Vince G. Brackett,[2] Marian B. Clayton,[2] Lorraine A. Brasseur,[2] David B. Harper,[2] Brian A. Ridley,[3] Andrzej A. Klonecki,[3] Peter G. Hess,[3] Louisa K. Emmons,[3] Xuexi Tie,[3] Elliot L. Atlas,[3] Christopher A. Cantrell,[3] Anthony J. Wimmers,[4] Donald R. Blake,[5] Michael T. Coffey,[3] James W. Hannigan,[3] Jack E. Dibb,[6] Robert W. Talbot,[6] Frank Flocke,[3] Andrew J. Weinheimer,[3] Alan Fried,[3] Bryan Wert,[3] Julie A. Snow,[7] and Barry L. Lefer[3]

[1] Ozone (O_3) and aerosol scattering ratio profiles were obtained from airborne lidar measurements on thirty-eight flights over seven deployments covering the latitudes of $40°-85°N$ between 4 February and 23 May 2000 as part of the Tropospheric Ozone Production about the Spring Equinox (TOPSE) field experiment. Each deployment started from Broomfield, Colorado, with bases in Churchill, Canada, and on most deployments, Thule Air Base, Greenland. Nadir and zenith lidar O_3 measurements were combined with in situ O_3 measurements to produce vertically continuous O_3 profiles from near the surface to above the tropopause. Potential vorticity (PV) distributions along the flight track were obtained from several different meteorological analyses. Ozone, aerosol, and PV distributions were used together to identify the presence of pollution plumes and stratospheric intrusions. Ozone was found to increase in the middle free troposphere ($4-6$ km) at high latitudes ($60°-85°N$) by an average of 4.6 ppbv/mo (parts per billion by volume per month) from about 54 ppbv in early February to over 72 ppbv in mid-May. The average aerosol scattering ratios at 1064 nm in the same region increased rapidly at an average rate of 0.36/mo from about 0.38 to over 1.7. Ozone and aerosol scattering were highly correlated over the entire field experiment, and PV and beryllium (^7Be) showed no significant positive trend over the same period. The primary cause of the observed O_3 increase in the mid troposphere at high latitudes was determined to be the photochemical production of O_3 in pollution plumes with less than 20% of the increase from stratospherically-derived O_3. *INDEX TERMS:* 0365 Atmospheric Composition and Structure: Troposphere—composition and chemistry; 3362 Meteorology and Atmospheric Dynamics: Stratosphere/troposphere interactions; *KEYWORDS:* ozone, aerosols, springtime, Arctic, trends

[1]Atmospheric Sciences, NASA Langley Research Center, Hampton, Virginia, USA.

[2]Science Application International Corporation, Hampton, Virginia, USA.

[3]National Center for Atmospheric Research, Boulder, Colorado, USA.

[4]Department of Environmental Sciences, University of Virginia, Charlottesville, Virginia, USA.

[5]Department of Chemistry, University of California, Irvine, California, USA.

[6]Institute for the Study of Earth, Oceans, and Space, University of New Hampshire, Durham, New Hampshire, USA.

[7]Graduate School of Oceanography, University of Rhode Island, Rhode Island, USA.

1. Introduction

[2] *Monks* [2000] presented a summary of the seasonal variation of tropospheric O_3 flux for the northern hemisphere (NH) as reported in the literature. He discussed the large-scale O_3 increase that is generally observed in the NH from April to June and examined the evidence for the various contributions to this increase from stratosphere-troposphere exchange (STE) and photochemistry. He indicated that the understanding of the spring O_3 maximum and its formation mechanism is of fundamental importance to atmospheric science, and this was the underlying objective of the TOPSE (Tropospheric Ozone Production about the Spring Equinox) field experiment.

[3] A comprehensive review of STE is given in *Holton et al.* [1995], which discusses the global-scale processes associated with STE and the spatial and seasonal characteristics of the downward mass transport that leads to the spring maximum in STE. Holton et al. present a globally averaged representation of potential temperature and potential vorticity (PV) which indicates that the major region for isentropic STE would be south of about 45°N with a relatively unchanging tropopause height and less downward transport north of 45°N. *Appenzeller et al.* [1996] modeled global-scale meridional circulations and seasonal variations in the mass of the lowermost stratosphere to estimate the net mass flux across the tropopause, and they found that in the NH, the flux showed a late spring maximum and autumn minimum. A recent study by *Seo and Bowman* [2001] examined cross-tropopause exchange, and they found that the downward exchange regions were well correlated with NH storm tracks. The maximum in STE mass transport at 330 K in the March–May period was centered near 35°N over the Pacific Ocean and over the southeastern United States, and most of the STE mass transport was south of 45°N, which is consistent with the general concept presented by *Holton et al.* [1995].

[4] Surface measurements of tropospheric O_3 were made at high latitudes over the Finnish Lapland (179–566 m ASL) in 1992 and 1993, and *Rummukainen et al.* [1996] found that O_3 peaked in May of each year, with the minimum observed from October to December. They also found that the contribution from the Atlantic Ocean was highest in winter and lowest in autumn, based on 5-day backward trajectories. However, since the backward trajectories were limited to 5 days, changes in the contributions from Eurasia during the year were difficult to discern. *Solberg et al.* [1997b] monitored O_3 at several Norwegian monitoring sites (3–500 m ASL) from 1989 to 1994, and again, O_3 was found to peak in May but was lowest around August. When they compared seasonal cycles of O_3 for stations from 58°23′N to 69°27′N, they found that at the southern stations, the O_3 peaked over background levels in July but at the northern stations, the peak occurred in May. An O_3 deficit was found during the winter months, and in the springtime, they speculated that net O_3 production proceeded slowly, and thus the O_3 change was most pronounced at the farthest distances from the NO_x sources. In the summer, they thought that the net production rates were higher, so the O_3 change would be found nearer to the NO_x sources.

[5] *Penkett and Brice* [1986] were the first to suggest that the springtime maximum in O_3 may be due to photochemistry. Seasonal changes in PAN in the UK were used to distinguish between contributions in tropospheric photochemistry and stratosphere-troposphere exchange. More recent observations of PAN at Zeppelin Mountain (474 m ASL), Norway (78°55′N, 11°54′E), were found to peak in March/April 1994, while non-methane hydrocarbons peaked in January/February [*Solberg et al.*, 1997a]. Thus, some of the important O_3 and PAN precursors have peak concentrations in winter or spring, then decrease, supporting the hypothesis that photochemical production of O_3 and PAN is important in the Arctic in the spring [*Penkett and Brice*, 1986]. *Wang et al.* [1998] presented model results for tropospheric O_3 production and loss, and they showed that

for high northern latitudes, transport from the stratosphere is larger than tropospheric photochemical production in January, but less in April and much less in July and October. Their model indicated that for Goose Bay (53°N, 60°W at 800 mb) the crossover point for the tropospheric contribution surpassing the stratospheric contribution occurred in April, and the tropospheric contribution continued to increase until it peaked in June.

[6] The TOPSE field experiment was conducted at high-latitudes over North America from 4 February to 23 May 2000 to investigate the cause of the springtime maximum in tropospheric O_3 [*Atlas et al.*, 2003]. Seven deployments were conducted with the NCAR (National Center for Atmospheric Research) C-130 aircraft during TOPSE, and they started and ended at NCAR's Research Aviation Facility at Jefferson County Airport in Broomfield, CO (39°55′N, 105°07′W). Each deployment consisted of flights through Winnipeg, Manitoba, Canada (49°53′N, 97°09′W) to Churchill, Manitoba, Canada (58°47′N, 94°12′W) and then north to Thule, Greenland (76°32′N, 68°45′W) on five of the seven deployments. Several deployments included local flights out of Churchill and Thule with the coverage extending to about 85°N near Alert, Nunavut, Canada (82°30′N, 62°20′W). Thirty-eight science flights were made during these deployments between 4 February and 23 May 2000. Most flights consisted of slow ascents to an altitude near 6–7 km with several slow spirals and/or stair step descents to sample vertical profiles with the in-situ instruments. Some flights also included low-level legs over the Hudson Bay and Alert near the end or beginning of flights from Churchill and Thule.

[7] This paper discusses the trends in O_3, aerosols, and trace gases observed in the free troposphere at high latitudes during TOPSE and relates these trends to changes found in PV, stratospheric-tropospheric exchange, tropospheric transport, and photochemical O_3 production.

2. Instrumentation and Methodology

[8] The NASA Langley Research Center's UV airborne differential absorption lidar (UV DIAL) system was flown on the NCAR C-130 aircraft for remote measurements of O_3 and aerosols across the troposphere and into the lower stratosphere. Various versions of the UV DIAL system have been used since 1980 for global and regional scale investigations of O_3 and aerosol distributions in the troposphere and lower stratosphere [see, e.g., *Browell*, 1989; *Browell et al.*, 1992, 1996a, 1998, 2001]. The airborne UV DIAL system used during TOPSE was previously described by *Browell* [1989], and this version of the UV DIAL system was last used in the TRACE-A (Transport and Atmospheric Chemistry Near the Equator-Atlantic) field experiment to study the impact of photochemical O_3 production from biomass burning on the O_3 budget over the tropical South Atlantic [*Browell et al.*, 1996b]. This version of the UV DIAL system was flown on the C-130 during TOPSE while a later version was being flown on the NASA DC-8 aircraft in the Arctic as part of the SAGE-III Ozone Loss and Validation Experiment (SOLVE) [*Schoeberl et al.*, 2002; W. B. Grant et al., Use of ozone distributions, potential vorticity, and cooling rates to estimate Arctic polar vortex
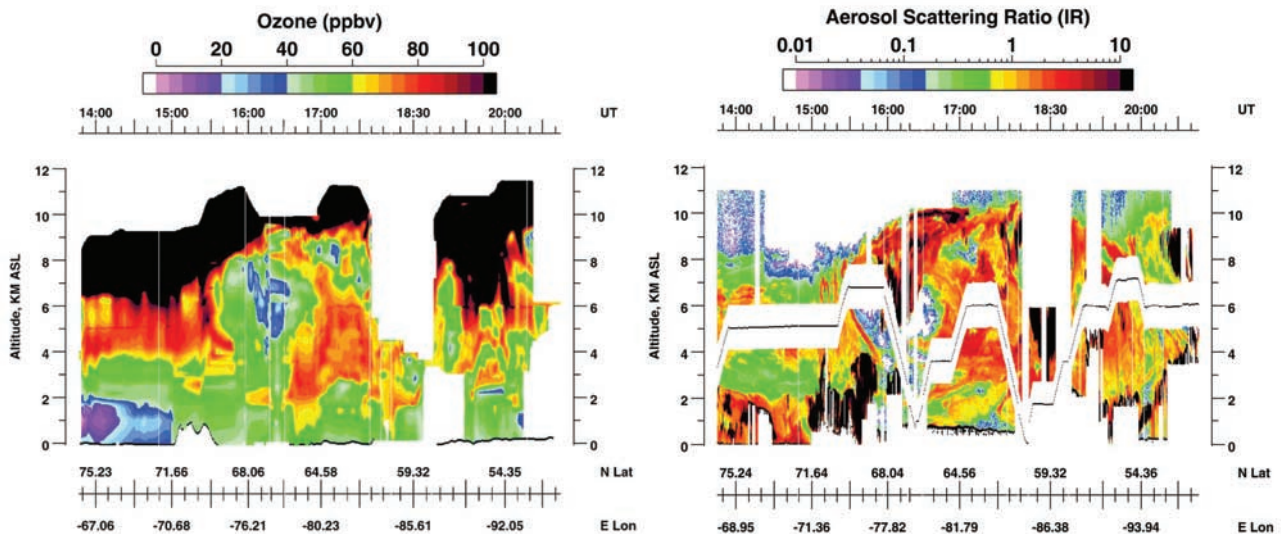
Figure 1. Ozone and aerosol scattering ratio distributions obtained on flight from Thule, Greenland to Winnipeg, Canada on 22 May 2000 (Flight 41). Aircraft flight altitude is shown on the aerosol plot as a continuous black line. In situ O_3 measurements are used to constrain and interpolate the DIAL O_3 data across the near-field range above and below the aircraft (shown as white on aerosol plot) where DIAL measurements are not made.

ozone loss during the winter of 1999/2000, manuscript submitted to *Journal of Geophysical Research*, 2002].

[9] The airborne UV DIAL system used during TOPSE operated at 8.6 Hz with two frequency-doubled Nd:YAG lasers pumping two dye lasers that were frequency-doubled into the UV to produce the on-line (288.2 nm) and off-line (299.6 nm) wavelengths for the DIAL O_3 measurements. The residual 1064-nm and ~590-nm beams from the frequency-doubling process of the Nd:YAG and dye lasers, respectively, were also transmitted with the UV wavelengths. As a result, four laser beams are transmitted simultaneously into the atmosphere below (288.2, 299.6, 576.4, and 1064 nm) and above (288.2, 299.6, 599.2, and 1064 nm) the aircraft for lidar measurements of O_3, aerosols, and clouds from near the surface to about 3 km above the tropopause. The average energy in each UV (288.2 or 299.6 nm), VIS (576.4 or 599.2 nm), and IR (1064 nm) laser beam was about 10–15, 40, and 150 mJ, respectively. The different lidar backscatter returns at the different wavelengths were dichroically separated in the separate nadir and zenith receiver systems, directed through tuned optical filters, and detected by optimized detector systems. The DIAL UV beams were transmitted with 300-μs separation so the UV lidar returns would be detected sequentially by the same photomultiplier tube. Real-time processing of the DIAL O_3 and aerosol data permitted optimizing the in situ sampling by the other instruments on the C-130.

[10] This system is used to measure O_3 and aerosol distributions starting at a distance of about 1 km above and below the aircraft and extending to a range of about 7 km in each direction. This enables measurements of nearly continuous O_3 and aerosol profiles from near the surface to several kilometers above the tropopause along the flight track of the aircraft. The accuracy of the UV DIAL measurements of O_3 with a vertical resolution of 300 m

and an averaging time of 5 minutes (about 38-km horizontal resolution at C-130 ground speeds) has been previously demonstrated to be better than 10% or 2 ppbv, whichever is greater, with a measurement precision of 5% or 1 ppbv [*Browell et al.*, 1983]. Intercomparisons between in situ and UV DIAL O_3 measurements were made throughout the course of TOPSE to ensure that the accuracy of the measurements was being maintained. The aerosol scattering ratio distributions are determined from the relative lidar backscattering distribution using standard atmosphere densities [*Jursa*, 1985] interpolated by month, latitude, and altitude along the flight track and a normalization of the lidar backscatter distribution to a clean (nearly aerosol free) region, usually found near the tropopause. The vertical and horizontal resolutions for the aerosol scattering ratio measurements are 30 m and 3.8 km (30-s averaging time).

[11] The in situ O_3 measurements on the C-130 [*Ridley et al.*, 2003] were used to constrain the interpolation of the O_3 distribution between the nadir and zenith UV DIAL measurements to produce an estimate of the O_3 distribution across the near-field region not covered by the UV DIAL measurements. In addition, the in situ O_3 measurements made below about 500 m were used to help estimate the extrapolated O_3 distribution from the lowest DIAL measurement altitude to the surface. These techniques have been used previously [*Fenn et al.*, 1999; *Browell et al.*, 2001] to obtain an estimate of the entire O_3 profile from the surface to above the tropopause. Figure 1 shows an example of the O_3 and aerosol scattering (S_A-IR) data obtained on TOPSE Flight 41 from Thule, Greenland to Winnipeg, Canada.

[12] Ozone and S_A data from each flight were binned into 0.25-degree latitudinal bins and averaged to arrive at the average latitudinal distribution for O_3 and S_A for each flight. To ensure we did not include aerosol scattering from clouds

or highly attenuated aerosol data on the far side of clouds, we used $S_A \geq 10$ to define a cloud, and we eliminated any aerosol data beyond a distance of 100 m in front of where a cloud was detected in either the nadir or zenith aerosol profile. The latitudinal O_3 and S_A distributions below the tropopause (determined from O_3 DIAL data [*Browell et al.*, 1996b]) from each flight were combined with the other flights in a deployment to produce an overall latitudinal distribution for O_3 and S_A for the deployment. In this process, the data were averaged together when the flights had overlapping data in the same latitudinal bin. The overall O_3 and S_A trends observed during TOPSE are derived from these deployment-average latitudinal distributions.

[13] Three different analyses were used to generate the PV distributions used in this investigation: the MRF (Medium Range Forecast) analysis from the University of Virginia [*Kanamitsu*, 1989; *Kanamitsu et al.*, 1991; *Iredell and Caplan*, 1997; *Caplan and Pan*, 2000]; the ECMWF analysis, which goes into the NCAR global chemical transport model, MOZART (Model for OZone And Related chemical Tracers) [*Brasseur et al.*, 1998; *Hauglustaine et al.*, 1998; *Emmons et al.*, 2003; *Tie et al.*, 2003]; and the MM5 (PSU/ NCAR Mesoscale Modeling System) analysis, which goes into the HANK (NCAR Regional, Chemical Transport) model [*Klonecki and Hess*, 2003; *Hess et al.*, 2000]. The MRF analysis is initialized with the data from the NCEP (National Center for Environmental Prediction) Global Data Assimilation System (GADS). MOZART was driven with ECMWF meteorological fields with a horizontal resolution of 2° and approximately 1-km vertical resolution [*European Centre for Medium-Range Weather Forecasts* (*ECMWF*), 1995], and the MOZART results provide the chemical boundary conditions for the regional HANK model. HANK's dynamics are based on fields calculated by the MM5 model [*Grell et al.*, 1993; see also *Klonecki and Hess*, 2003], and the meteorological initial and boundary conditions for the MM5 analysis were provided by the NCEP MRF (Medium Range Forecast) global model. The horizontal resolution of the HANK model is comparable to the MOZART model (243 km × 243 km at 60°N), however the vertical resolution is considerably higher with 39 levels between the surface and 100 mb. The details of each of these models and their underlying meteorological analysis are presented in their respective references. The MRF, HANK, and MOZART models provided interpolated, vertical cross sections of PV distributions along the flight track of the C-130 during TOPSE. These cross sections were handled in the same manner as the UV DIAL O_3 and S_A data to arrive at latitudinally binned data for each flight and then for each deployment. All PV cross sections were masked to correspond to the same altitude and geographic limitations as the UV DIAL O_3 data.

[14] Results from various in situ measurements made on the C-130 are also presented to provide insight into the cause of the trends observed in the O_3 measurements. *Atlas et al.* [2003] provide an overall description of the instrumentation on the C-130 and their respective references.

3. Results and Discussion

[15] Ozone and aerosol data were obtained with the UV DIAL and in situ instruments on the NCAR C-130 on all seven TOPSE deployments. An example of the UV DIAL O_3 and aerosol data with the in situ O_3 measurements imbedded in the O_3 cross section is shown in Figure 1. These data obtained on the flight from Thule to Winnipeg show the complexity of the atmospheric structure that was encountered on many of the TOPSE deployments. The tropopause is generally above an O_3 level of 100 ppbv, and at latitudes above 68°N, the tropopause was generally found to be above 7 km, while at lower latitudes it was above 10 km. During TOPSE, the aerosol loading in the lower stratosphere was low with an S_A-IR of ≤ 0.5. Evidence of an intrusion of stratospheric air can be seen in both the aerosol and O_3 data from ~1530 to ~1550 UT at 4.5– 6.0 km. In situ data also confirmed we passed through this tongue of stratospheric air, which was related to a jet stream crossing and its associated change in tropopause height [see, e.g., *Browell et al.*, 1987].

[16] Large regions with very high aerosol scattering ratios ($S_A \geq 1$) were observed throughout the troposphere at all latitudes but particularly south of 68°N. These regions also had elevated O_3 levels (≥ 70 ppbv) compared to the regions of low aerosol scattering ($S_A \leq 0.3$) (not including the stratospheric intrusion region), which had O_3 levels near 50 ppbv. The regions with correlated enhancements in aerosol scattering and O_3 are associated with continental pollution and photochemical O_3 production, which has been well documented in many previous airborne field experiments [see, e.g., *Browell et al.*, 1992, 1996a, 1996b].

[17] Clouds exhibit very enhanced aerosol scattering ($S_A > 10$), and the laser beams that get through the clouds are highly attenuated. Various low, mid-level, and high clouds can be seen on Figure 1. These clouds result from various meteorological processes with the clouds near the surface being of a local origin and the mid-level and high clouds resulting from long-range transport in the troposphere. A region of low O_3 (<30 ppbv) with enhanced aerosol scattering was observed near the surface (below 2 km) north of ~72°N. This region of low O_3 is thought to be caused by O_3 destruction due to bromine chemistry [*Ridley et al.*, 2003].

3.1. Ozone Trends

[18] The average latitudinal O_3 distributions for each deployment were derived from an average of the flight-binned O_3 data as previously discussed, and these distributions are shown in Figure 2. Most of the deployments covered the entire latitudinal range of 40°–85°N, but Deployments 1 and 3 did not extend beyond 67°N. In addition, Deployment 2 had no O_3 data in the region 45°–56°N due to extensive cloud cover. The general transition from free tropospheric O_3 levels in the range of 40–60 ppbv in the first three deployments to levels of 60– 80 ppbv by the last deployment is readily apparent in Figure 2. The low O_3 levels near the surface can be seen in all the average latitudinal distributions with a particularly large region north of 76°N on Deployment 6.

[19] To better quantify the trend in O_3 in the free troposphere, the data shown in Figure 2 were binned into two latitudinal regions (40°–60°N and 60°–85°N) and two altitude regions (2–4 km and 4–6 km). The average O_3 value and the standard error of the average are shown in
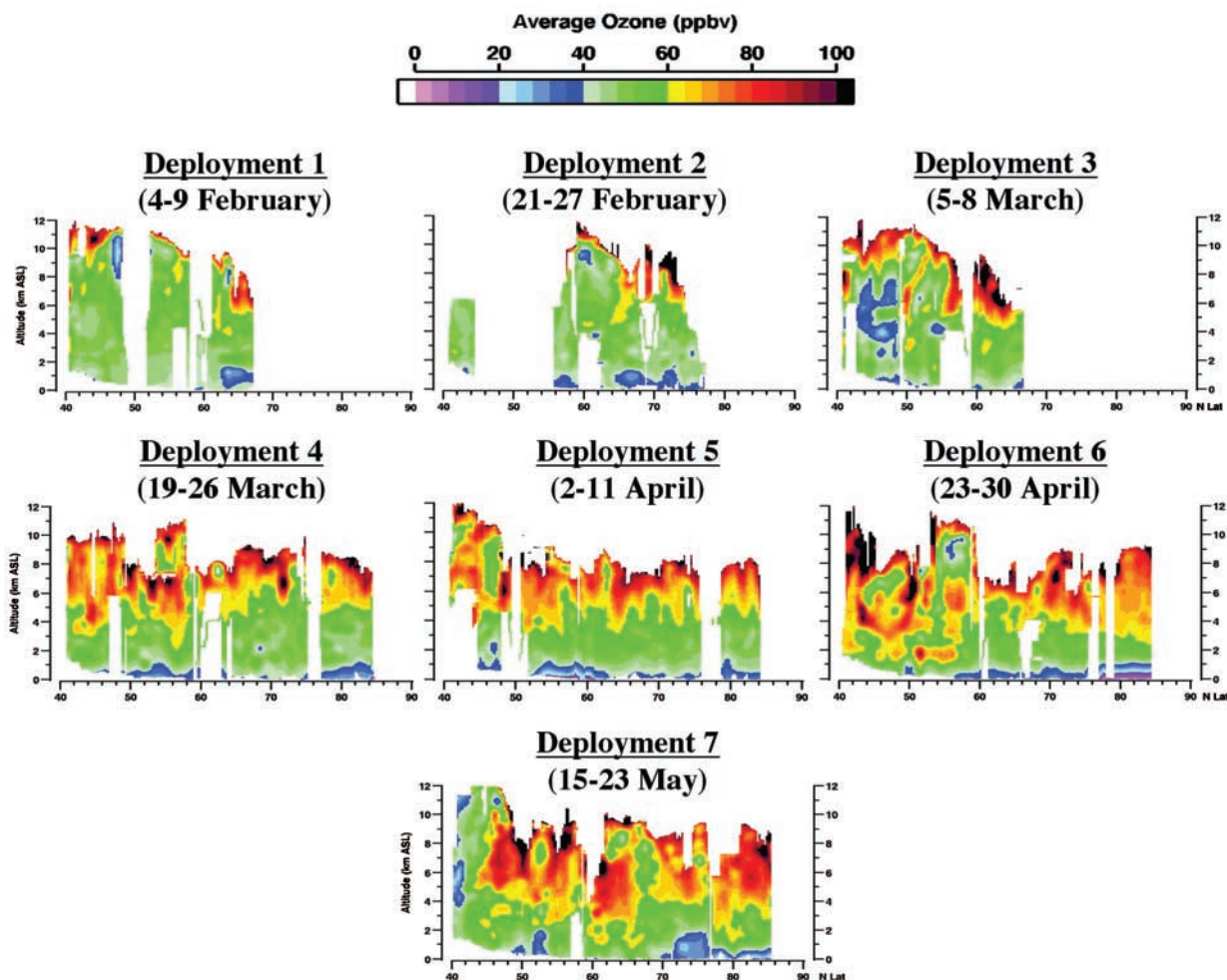
Figure 2. Average O_3 distributions observed on each deployment during TOPSE.

Figure 3 for each deployment in each region. A linear correlation for the first four deployments and the last four deployments as well as for the entire TOPSE field experiment are shown. In the fit, the deployment averages were weighted by the normal inverse of the variance of the standard error of the average in an attempt to account for the reduced latitudinal coverage and resulting larger measurement uncertainty in a few of the deployments as noted above. The slope of the overall correlation line and its standard deviation is also given in Figure 3 along with the correlation coefficient for the fit. The O_3 increased in all of the regions as was generally indicated from the data presented in Figure 2. The observed trends in O_3 were larger in both altitude regions at $40°-60°N$ compared to the respective altitude regions at $60°-85°N$ (see Figure 3). In the first three deployments at $40°-60°N$, O_3 was rather constant at $\sim$49 ppbv with very little vertical gradient. Starting in the fourth deployment, O_3 increased abruptly in the $4-6$ km region to $\sim$66 ppbv, and it stayed near that level for the rest of the field experiment. This transition was also seen in the $2-4$ km region, but the change was not as large.

[20] In the higher latitudinal region ($60°-85°N$), there was no similar abrupt increase in O_3 seen in the fourth deployment; in fact, it appears like there was no increase

at all during the first four deployments. Ozone steadily increased from the fourth to seventh deployments. The intermediate correlation fits show the break in the trends between the two periods. The O_3 value for Deployment 3 is the only outlier that does not follow this trend, and we believe that this is due to two factors: (1) the limited amount of data available north of $60°N$, and (2) the data that was collected was in the vicinity of a stratospheric intrusion, which is also reflected in the PV analyses for this deployment (to be discussed later). The average increase in O_3 over the TOPSE field experiment in the free troposphere was found to be 3.0 ppbv/mo at low altitudes ($2-4$ km) increasing to 4.6 ppbv/mo in the mid troposphere ($4-6$ km). Examining the trend over the final four deployments, the rate would be as large as 5.0 and 6.7 ppbv/mo, respectively, with very high correlation coefficients ($R > 0.96$).

3.2. Aerosol Trends

[21] The average latitudinal distributions of IR aerosol scattering ratios (S_A) were constructed for each deployment using the procedures discussed above. They were further limited to the same regions where the O_3 data existed for each deployment as shown in Figure 2. The resulting average latitudinal distributions of S_A for each deployment
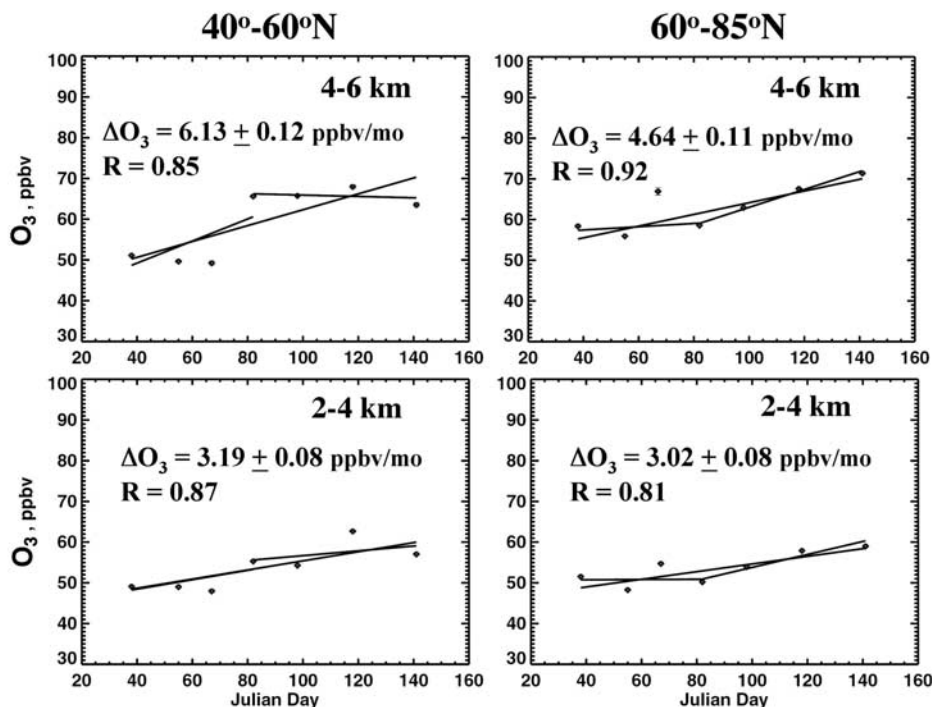
Figure 3. Average O_3 trends in different latitude and altitude regions. Note that the vertical bars, which represent the standard error of the O_3 average, are so small in most cases that they are obscured by the size of the symbol used to designate the average O_3 value.

are shown in Figure 4. The reason these distributions appear to be more limited than the O_3 distributions is due to the omission of aerosol data that are compromised due to clouds or cloud attenuation. The trend in aerosol scattering is more difficult to see in the figure, particularly in the first three deployments, but starting with the fourth deployment there is a general indication that the amount of aerosol scattering is increasing with time. To better quantify the changes in S_A over TOPSE, the aerosol data were binned in the same manner as the O_3, and this is shown in Figure 5.

[22] The scatter in the S_A values for the first three deployments was very large in all regions shown in Figure 5, with the possible exception of the $60°-85°N$, 4–6 km region where the scatter was low and the S_A trend for the first four deployments was consistent with the overall trend for the field experiment. In the $40°-60°N$ region, the S_A values increased very rapidly from the fourth to seventh deployments at all altitudes in the free troposphere. In the $60°-85°N$ region, there was no significant change in S_A values in the fourth to seventh deployments in the lower free troposphere, but in the 4–6 km region there continued to be an increase which could have even started in early February. The rate of increase in S_A in the $60°-85°N$, 4–6 km region was found to be 0.36/mo over the entire field experiment or 0.39/mo over the last four deployments. This compares to the $40°-60°N$, 4–6 km region with 0.54/mo overall and 0.86/mo over the last four deployments. The sulfate layer in the Artic stratosphere was observed during January and March 2000 as part of the SOLVE (SAGE-III Ozone Loss and Validation Experiment) field experiment to have a maximum S_A value of about 0.5 (E. V. Browell et al., manuscript in preparation, 2002), and thus the observed

increase in S_A in the troposphere could not have been due to the downward transport of stratospheric aerosols.

3.3. O_3/Aerosol Correlation

[23] Both O_3 and aerosol scattering were found to increase during TOPSE in all regions of the free troposphere from $40°-85°N$ (Figures 3 and 5 and higher altitude regions not shown in these figures), but to investigate whether they were increasing together, it is necessary to examine their correlation to each other. Figure 6 presents a representative correlation plot for O_3 and S_A for the $60°-85°N$, 4–6 km region (all of the other regions exhibit similar results). The deployment averages and the standard error of the averages for O_3 and S_A are shown along with the best fit linear correlation line and the correlation coefficient. The O_3 and S_A data from all the deployments show very good correlation (R = 0.95) with a positive regression slope of O_3/S_A = 10.6 ppbv and intercept of 54.4 ppbv. The high positive correlation between O_3 and aerosols is usually found in association with continental pollution plumes, which is opposite to the negative correlation between O_3 and aerosols that is found in association with stratospherically influenced air observed in the troposphere [*Browell et al.*, 1996a, 1996b].

3.4. Potential Vorticity Results

[24] Potential vorticity (PV) analysis associated with the MRF, HANK, and MOZART models were produced for the TOPSE period, and PV cross sections along the C-130 flight tracks were interpolated from the gridded PV data from each model. These results were binned and averaged for each flight and for each deployment in the same manner as
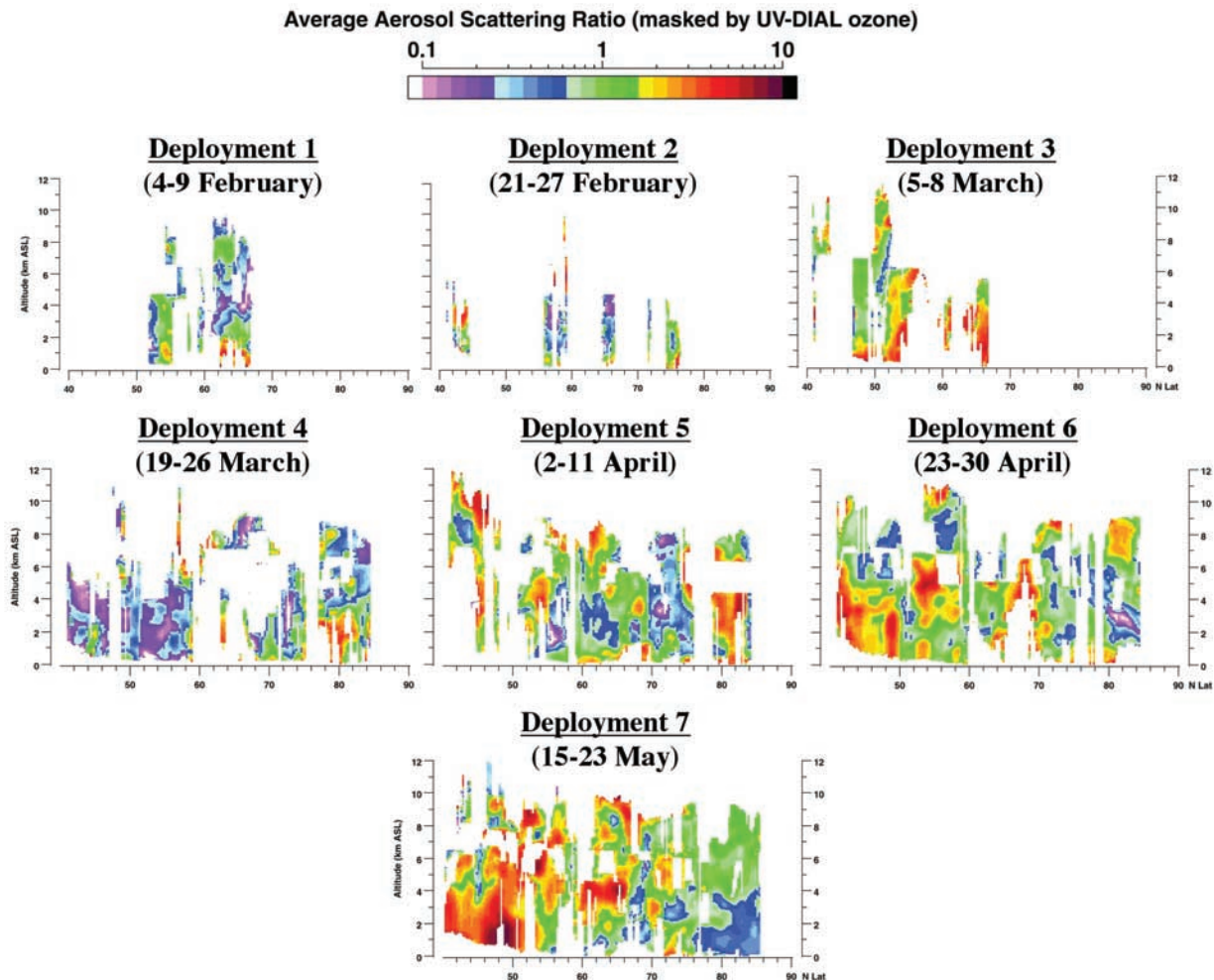
Figure 4. Average IR aerosol scattering ratio distributions observed on each deployment during TOPSE.

the O_3 and aerosol data. An initial comparison was made between the MRF PV results with and without the DIAL O_3 data masking to ensure the masking process did not produce biased PV results that were not supported by the unmasked PV data. An example of unmasked and masked MRF PV data for Deployment 4 is shown at the top of Figure 7. Note that for the unmasked case, the tropopause was assumed to be at PV = 2.5, and no PV values above the tropopause were included in the latitudinal PV average. In the masked case, the O_3 derived tropopause was used when available, but when not available, the above PV limit was used. While there are some differences between the unmasked and masked cases, particularly within about 1 km of the tropopause and south of about 65°N, the major features are preserved in the masked data. It was found that there were no significant differences in the PV trends between the masked and unmasked results, and since the masked data must be used to compare with the O_3 and aerosol measured trends, that is what was used in all the subsequent analysis.

[25] The PV distribution associated with the MOZART and HANK models for Deployment 4 is also shown for comparison with the MRF results in Figure 7. The MRF and HANK results appear to be very similar, and the MOZART

PV levels are generally lower in the free troposphere (2−8 km) and higher near the surface (<2 km), due to differences in the vertical resolution (coarser in the mid-troposphere and higher at the surface). Figure 8 examines the overall PV trends determined from the MRF analysis in the 2−4 km and 4−6 km altitude intervals in both the 40°−60°N and 60°−85°N regions. The lower latitude region has a PV average background level of about 0.4 PVU, where PVU = 10^{-7} K m^2 (kg s)$^{-1}$, while the PV background average at the higher latitudes is about twice as large. There is only a very slight increase in PV with altitude in the two latitudinal regions, and there is no statistically significant trend, either positive or negative, in PV in any of the regions over the entire TOPSE deployment. The high PV associated with Deployment 3 is due to the limited data in the 60°−85°N region having been collected in the vicinity of a stratospheric intrusion. Similar results (in general and for Deployment 3) for the 60°−85°N region are shown in Figure 9 from the HANK and MOZART models. The higher resolution HANK model had no trend at 2−4 km and the largest negative trend of any of the models at 4−6 km (ΔPV = −0.040 PVU/mo). The MOZART model showed a negative trend (ΔPV = −0.035 PVU/mo) in 4−6 km region and a
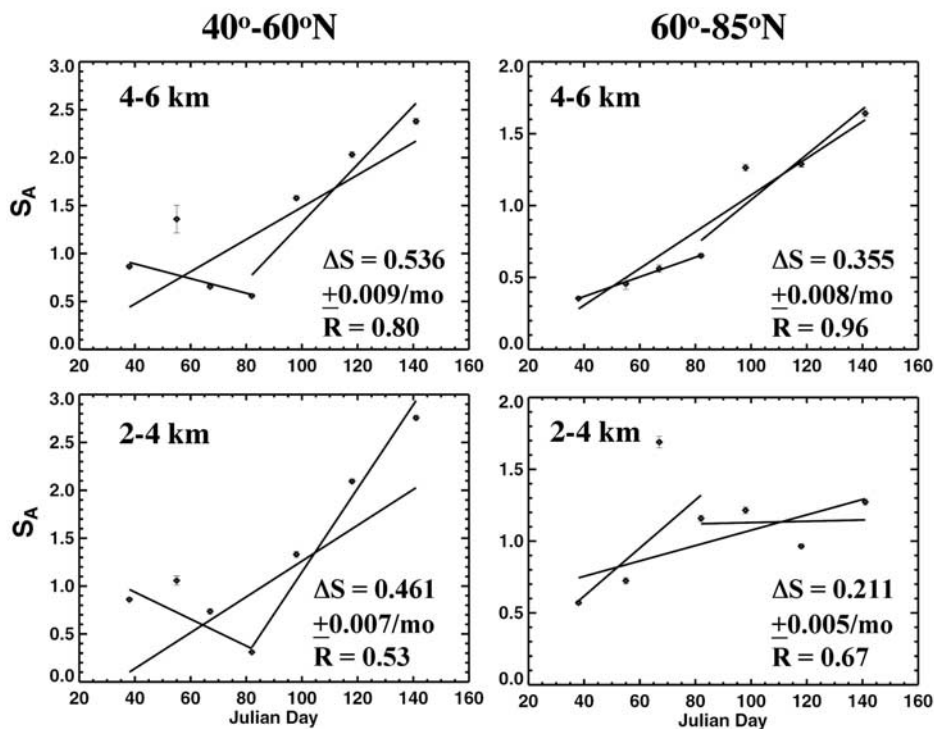
Figure 5. Average aerosol scattering ratio trends in different latitude and altitude regions.

similar negative trend in the lower altitude region. The correlation for the HANK and MOZART model results in the 60°–85°N region, while low, are more significant (based on correlation coefficient value) than the MRF results in this same region.

3.5. Calculated O_3 Based on PV and O_3/PV Ratio

[26] To estimate the contribution that stratospherically derived O_3 makes to the trend in tropospheric O_3, we combine the PV information previously discussed with the relationship between O_3 and PV in the lower stratosphere. The tropospheric PV levels and O_3/PV ratio in the lower stratosphere have been previously used to estimate the relative contribution that stratosphere-troposphere exchange makes relative to photochemistry in determining tropospheric O_3 amounts [*Browell et al.*, 1996a, 1996b, 2001; *Fenn et al.*, 1999]. A. A. Klonecki et al. (Analysis of the correlation between O_3 and potential vorticity in the lower stratosphere and possible applications, submitted to *Journal Geophysical Research*, 2002) have recently discussed the temporal variation in O_3 and PV across the stratosphere from extensive ozonesonde data from many sites. We used their time-dependent average O_3/PV relationship in the lower stratosphere (PV = 7) (see Table 1) and applied it to the PV distribution obtained from the various models across the TOPSE field experiment. In addition, for comparison we also applied the time-dependent O_3/PV ratio found in the lower stratosphere above Resolute, Northwest Territories, Canada (74.7°N, 95.0°W) (see Table 1). The results are shown in Figure 10. Based on the background value of PV in the troposphere in early February and the average stratospheric O_3/PV ratio at that time, the background amount of O_3 that could be attributed to a strato-

spheric source was over 73% of the observed background O_3 level for MRF, 84% for HANK, and 62% for MOZART. This shows the large influence of stratosphere-troposphere exchange on the background O_3 level in the late winter in this region. The stratospherically derived O_3, which was calculated from the PV results from HANK and MOZART, showed an overall negative trend using the average O_3/PV ratios and no trend using the Resolute O_3/PV ratios. Only the MRF results showed any overall positive tendency with a slope of 0.39 ppbv/mo using the global average O_3/PV
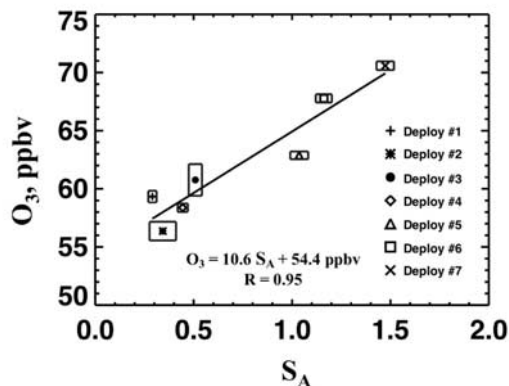

Figure 6. Correlation between O_3 and IR aerosol scattering ratios during TOPSE in mid troposphere (4–6 km) and at high latitudes (60°–85°N). Size of rectangles represents the standard error in the mean value of O_3 and aerosol scattering ratios for each deployment.
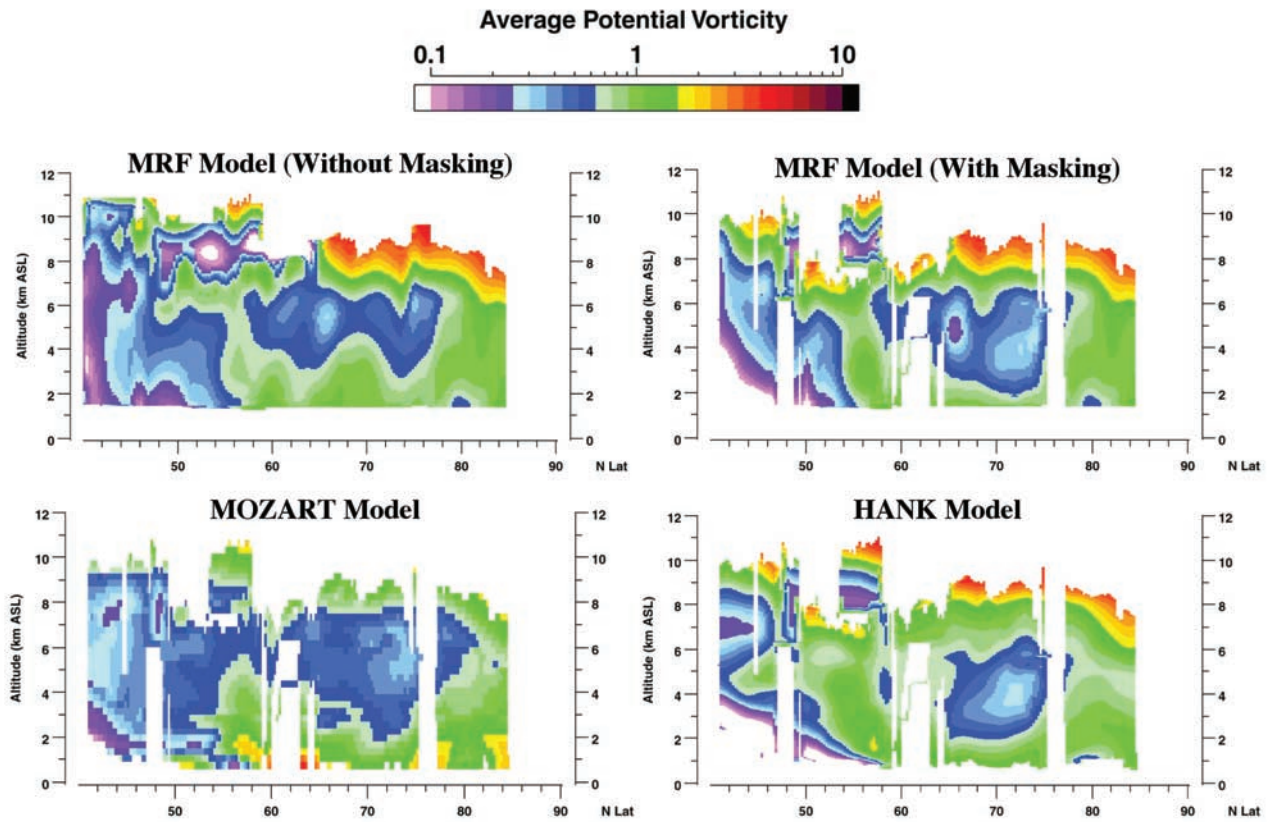
Figure 7. Average PV distributions for TOPSE Deployment #4 (19–26 March 2000) from MRF Model (with and without masking with UV DIAL O_3 data) and MOZART and HANK Models (both with UV DIAL O_3 data masking).
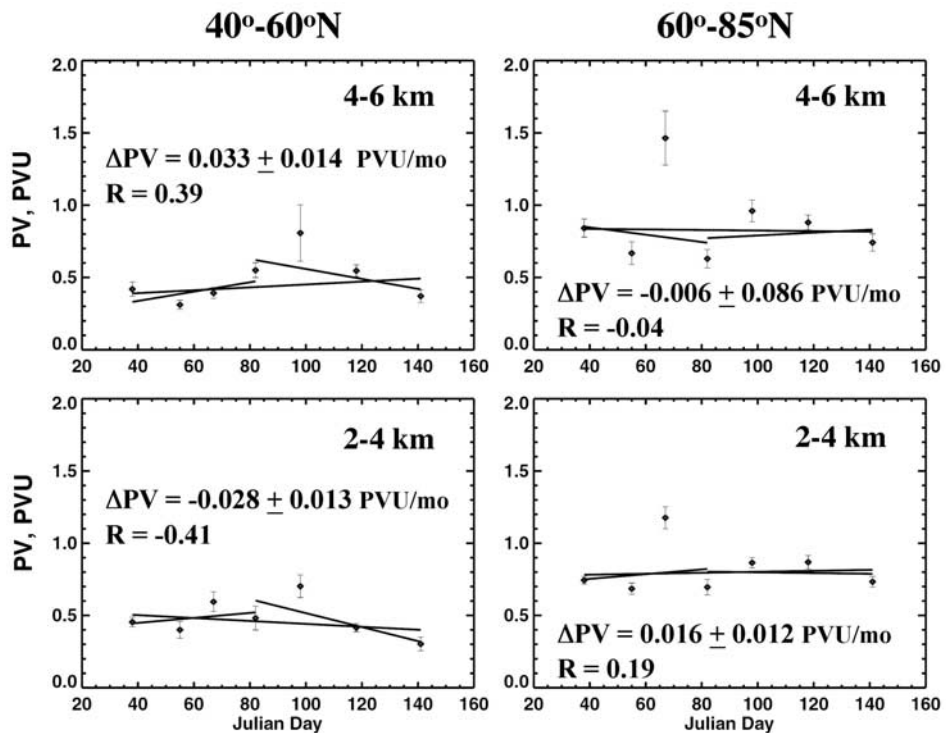

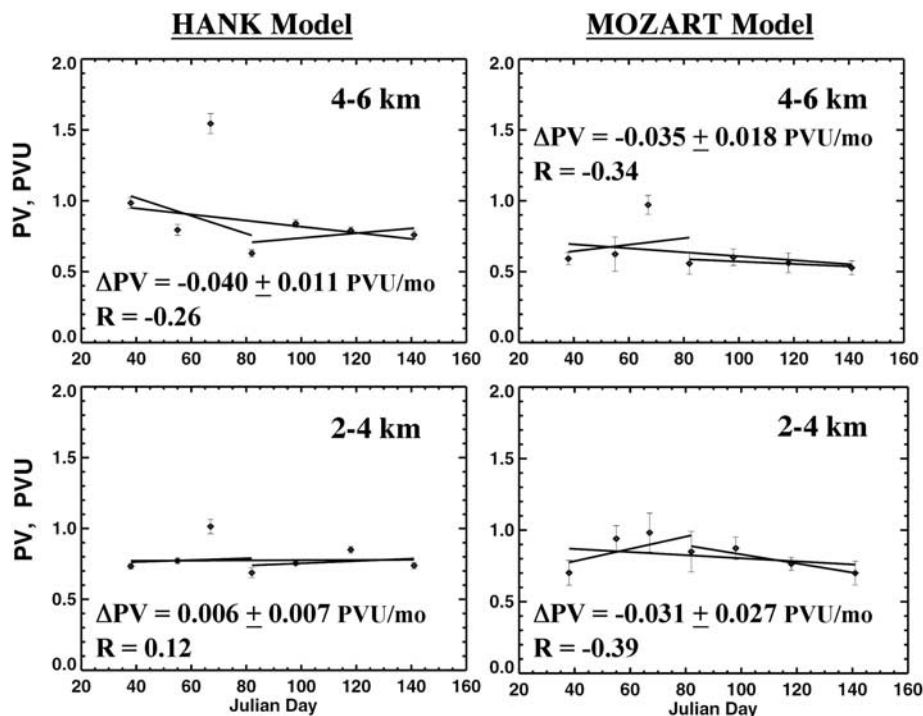**Figure 8.** MRF PV trends in different latitude and altitude regions.

Figure 9.   HANK and MOZART PV trends in 60°–85°N region.

ratios and 2.8 ppbv/mo using the Resolute ratios; however, regardless of which O_3/PV ratios are used, there was a strong negative trend in the MRF data during the last three deployments at the same time as there was a definite increase in the observed O_3 and aerosols across this region. It should be noted that the high O_3 values calculated in all the models for the third deployment were due to the samples being limited to the vicinity of a stratospheric intrusion and the spatial differences in the modeled versus observed intrusion location.

3.6.   Comparison of MOZART and Observed Ozone

[27]   Figure 11 presents the O_3 trends from the MOZART model in comparison with the observed O_3 trends in the 60°–85°N region. The trend in O_3 from the MOZART model at the lower altitudes is a factor of two higher than was observed. While the O_3 concentration predicted for the end of TOPSE was close to that observed, we did not observe the very low average O_3 levels (<40 ppbv) indicated by MOZART at the beginning of TOPSE - thus the differences in the overall predicted and observed trends at low altitudes in the free troposphere. At higher altitudes in the free troposphere (4–6 km), the overall trends were more comparable to the modeled average O_3 levels, which were slightly lower at the start of TOPSE than the observed values, but at the end of TOPSE the levels of O_3 were very close. The trend in the observed O_3 levels between the fourth and seventh deployments of 6.7 ppbv/mo is the same as what the MOZART model was indicating for the entire field experiment. It should be noted that the MOZART O_3 trend when it is not masked with the UV DIAL data is only slightly lower at 6.5 ppbv/mo. This shows that there was very little bias in using the data only in regions where the

UV DIAL O_3 measurements were made. The amount of stratospheric O_3 at 60°–85°N, 4–6 km, as derived from MOZART/ECMWF PV, was about 35–40 ppbv throughout the campaign (Figure 10). However, the total simulated O_3 from MOZART increased through the spring (Figure 11), implying the increase was caused by tropospheric chemical production (either locally or transported from outside the region). This conclusion is consistent with the results discussed in the previous section and those presented by *Emmons et al.* [2003].

### 3.7.   Long-Range Transport of Air to High Latitudes

[28]   To investigate the source of the air reaching the TOPSE experiment region in the mid troposphere, we used 10-day backward isentropic trajectories for air masses reaching the TOPSE flight tracks at altitudes from 4 to 6 km. Several examples from different deployments are shown in Figure 12. The one for 25 February (Flight 12 in Deployment 2) indicates that the air masses we observed spent much of the previous 10 days over the Pacific Ocean,

Table 1.   Lower Stratospheric Values of O_3/PV

Month	Center of Month Day Number	Average O_3/PV at PV = 7 (~200 mb)[a] (ppbv/PVU)	Resolute O_3/PV at PV ~ 5.5 (280 mb) (ppbv/PVU)
January	15	53.3	38
February	45	66.0	50
March	74	70.0	52
April	105	72.2	57
May	135	67.4	62
June	166	58.5	52

[a]From Klonecki et al. (submitted manuscript, 2002).

Ozone Using Time-Dependent Average O₃/PV Ratio at Many Sites
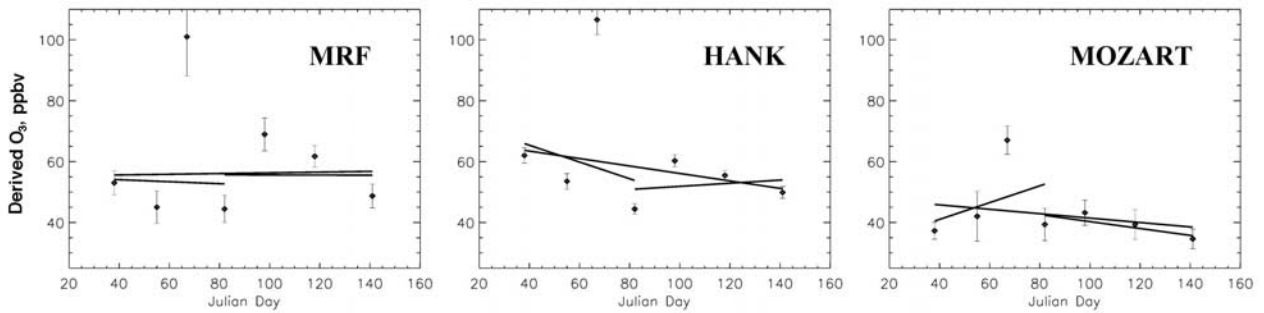
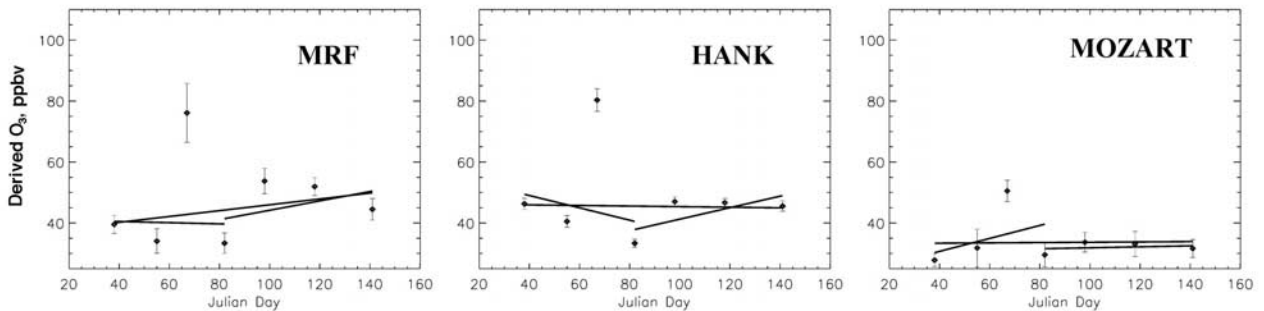## Ozone Using Time-Dependent O₃/PV Ratio at Resolute (75°N/95°W)

Figure 10. Ozone trend in $60°-85°N$, $4-6$ km region calculated from PV $\times$ O₃/PV, where PV is derived from MRF, HANK, and MOZART models, and O₃/PV is from the time-dependent average O₃/PV ratio in lower stratosphere (PV = 7 PVU) (Klonecki et al., submitted manuscript, 2002) (upper plots) and from the O₃/PV ratio from Resolute (280 mb, PV = 5-6 PVU) (lower plots).
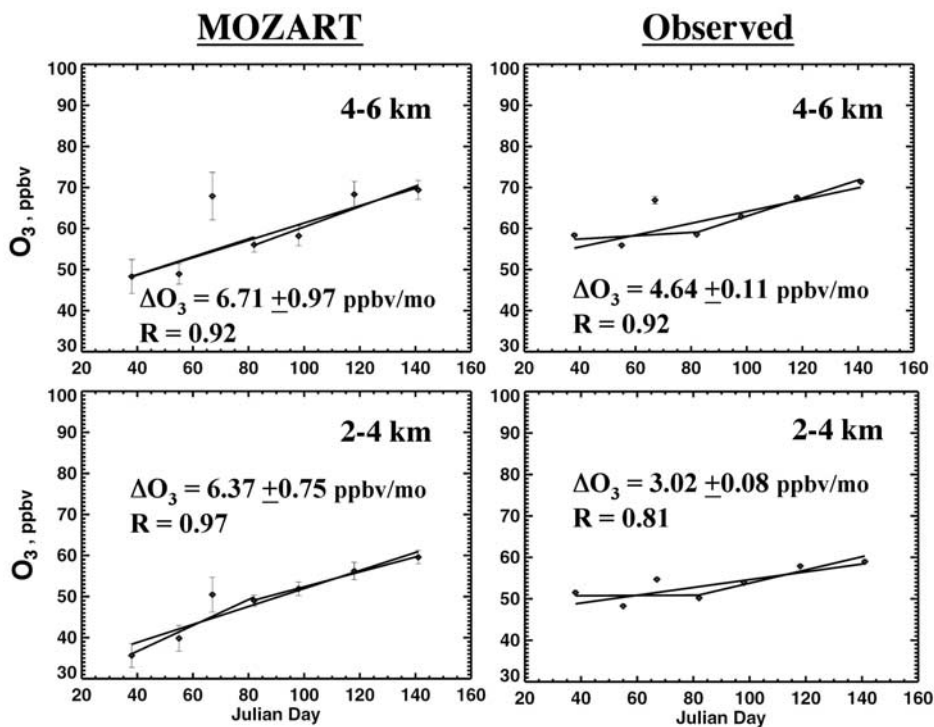

Figure 11. Comparison of MOZART and observed O₃ trends in $60°-85°N$ region.
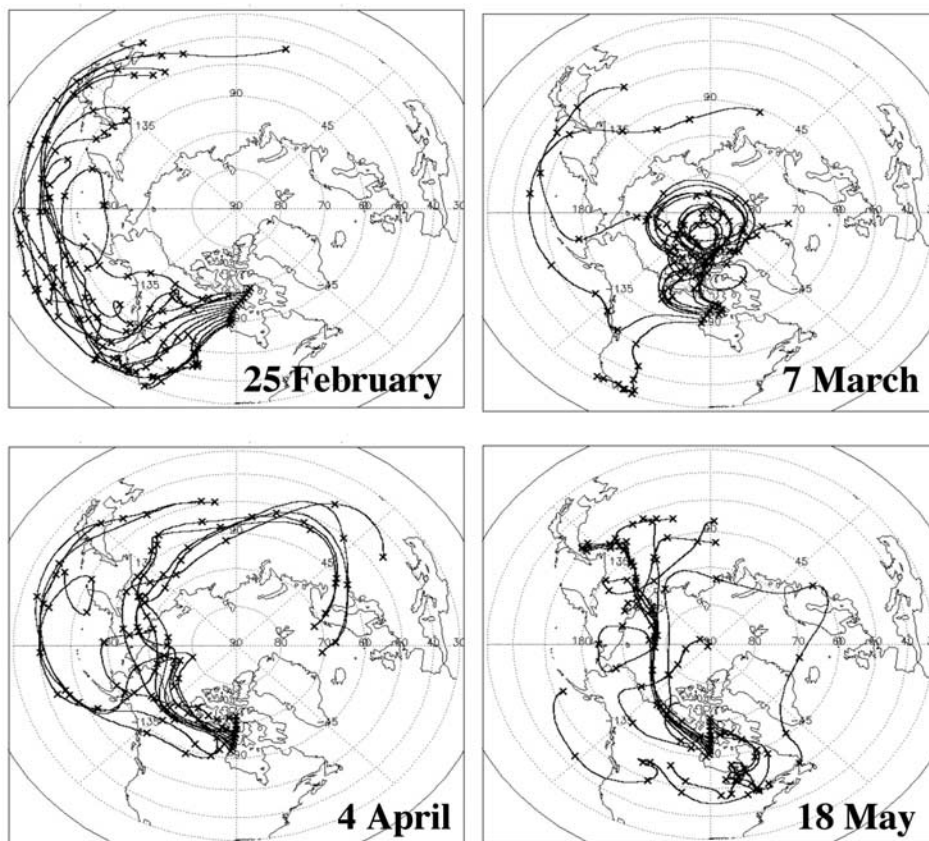
Figure 12. Ten-day backward trajectories from portions of TOPSE flight at altitudes of 4−6 km.

having originated in East Asia approximately 10 days earlier. The backward trajectories also show that a number of the air masses were within 2 km of the ocean surface, then rose to near 6 km after crossing the coast. When the air masses spend long times over oceans, the O_3 precursors can react and become diluted. While there was some transport over the United States for 25 February, it was not a period of high-activity photochemistry, and only a small fraction of the backward trajectories traversed urban/industrial areas. The 7 March (Flight 16 in Deployment 3) set of backward trajectories indicates that the air was generally confined to the Arctic for the previous 10 days. The backward trajectories for 4 April (Flight 26 in Deployment 5) and 18 May (Flight 39 in Deployment 7) show that for this period, the air masses reached the flight tracks 5−7 days after leaving Asia or Europe, regions with large emissions of O_3 precursors, and that the southern latitudes reached during transit were as low as 40°N, where considerable photochemical processing could occur.

[29] An assessment was conducted to determine the fraction of the time the air mass backward trajectories, ending in the 60°−85°N, 4−6 km region, were over different source regions during the previous 6−10 day period and below 4 km at some time during the same period. Table 2 presents a summary of these results. The low-altitude (<4 km) source region during the first four deployments was dominated by the Pacific Ocean. As mentioned above, this would generally be the source region for the cleanest air masses. During the last four deployments, the combination

of a rapidly decreasing Oceanic source and a rapidly increasing Continental (US/Canada and Eurasia) source is evident. In particular, Eurasia dominated the low-altitude source region in the last two deployments. With the exception of Deployment 3, which was discussed previously, there is a general increasing trend in ascending backward trajectories that come from Continental source regions during TOPSE. Prior literature indicates similar results for long-range transport into the Arctic. For example, *Pacyna and Oehme* [1988] show some transport to the Arctic from Eurasia in mid-March; *Bridgman et al.* [1989] show transport from Europe to Point Barrow, Alaska in early April; and *Djupstrom et al.* [1993] show transport from Eurasia to the high Arctic in early April.

[30] To examine the potential impact of descending air masses that might be associated with STE, the fraction of

Table 2. Fraction of Backward Trajectories With Ascent From Below 4 km Into 60°−85°N, 4−6 km Region

Backward Trajectory Source Region (Day 6−10)	Deployment Number						
	1	2	3	4	5	6	7
Arctic (>60°N)	0.00	0.02	0.00	0.06	0.20	0.08	0.05
Pacific Ocean	0.10	0.31	0.16	0.49	0.15	0.09	0.03
Atlantic Ocean	0.01	0.02	0.00	0.03	0.08	0.04	0.02
US/Canada	0.03	0.04	0.11	0.02	0.09	0.02	0.08
Eurasia	0.03	0.03	0.00	0.02	0.02	0.12	0.10
Total oceanic	0.11	0.33	0.16	0.52	0.23	0.13	0.05
Total continental	0.06	0.07	0.11	0.04	0.11	0.14	0.18

Table 3. Fraction of Backward Trajectories With Descent From Above 8 km Into $60°-85°N$, $4-6$ km Region

Starting Point of Backward Trajectory	Deployment Number						
	1	2	3	4	5	6	7
10 Days Prior	0.13	0.07	0.44	0.02	0.02	0.12	0.01
5 Days Prior	0.00	0.00	0.19	0.00	0.02	0.05	0.00

backward trajectories that descended from above 8 km into the $60°-85°N$, $4-6$ km region was determined for each deployment. Table 3 shows these results for end points of the backward trajectories at 10 and 5 days prior. Deployment 3 was strongly influenced by descending air in association with a stratospheric intrusion, and this is also reflected in the large fraction of descending backward trajectories at both 10 and 5 days prior. While there are a few descending trajectories in nearly all the deployments, there is no apparent trend associated with an increase in descending air during TOPSE. In fact, except for a slight increase associated with Deployment 6, the last four deployments have the lowest numbers of backward trajectories that exhibit descent (<2%) of the entire TOPSE campaign with Deployment 7 having the lowest levels of all (<1%).

[31] All of the above long-range transport results further support the hypothesis that most of the O_3 trend observed during TOPSE was from photochemical production in air from continental sources and not from an increase in STE.

3.8. Trace Gas and Aerosol Trends

[32] Key trace gases and aerosols were measured in situ on the C-130 during TOPSE, and their observed trends over this field experiment were used to further investigate the relative contribution of photochemistry and stratosphere-troposphere exchange in determining the O_3 trends across the spring equinox at high latitudes in the mid troposphere. The results from the average in situ O_3 measurements are shown in Figure 13, and they indicate an overall increase of 6.8 ppbv/mo, which is nearly identical to the predicted trend from the MOZART model, and very close to the 6.7 ppbv/mo seen in the last four deployments from the combined UV DIAL and in situ O_3 distributions. The in situ measurements of aerosol number densities in the $0.1-3.0$ μm range are also shown in the figure, and the aerosol number density trend reflects the same strong positive trend as was observed in the aerosol scattering data presented in Figure 5. PAN is a strong indicator of in situ tropospheric photochemistry, and it has a strong positive trend across the entire field experiment (Figure 13), which was also found by F. Flocke et al. (Measurements of PAN and PPN, and the budget of reactive oxidized nitrogen during TOPSE, manuscript submitted to Journal of Geophysical Research, 2002).

[33] As an indicator of stratospheric air, ^7Be should show a significant positive trend if the stratosphere-troposphere exchange was increasing over this period of time, but the ^7Be data showed only a small (9.8 fCi m^{-3}/mo) positive trend over TOPSE. Note that the ^7Be trend determination used an inverse weighting by the standard deviation of the ^7Be measurements (shown in Figure 13) due to the small number of independent observations $(3-17)$ in the target region during each deployment. Using an average value of 0.058 ppbv/fCi m^{-3} for the ratio of O_3/^7Be in the lower stratosphere, which was derived from measurements of O_3 and ^7Be in the lower stratosphere at $O_3 \geq 150$ ppbv [*Dibb et al.*, 2003], the trend in stratospherically-derived O_3 as indicated by the trend in ^7Be was determined to be 0.57 ppbv/mo. The above
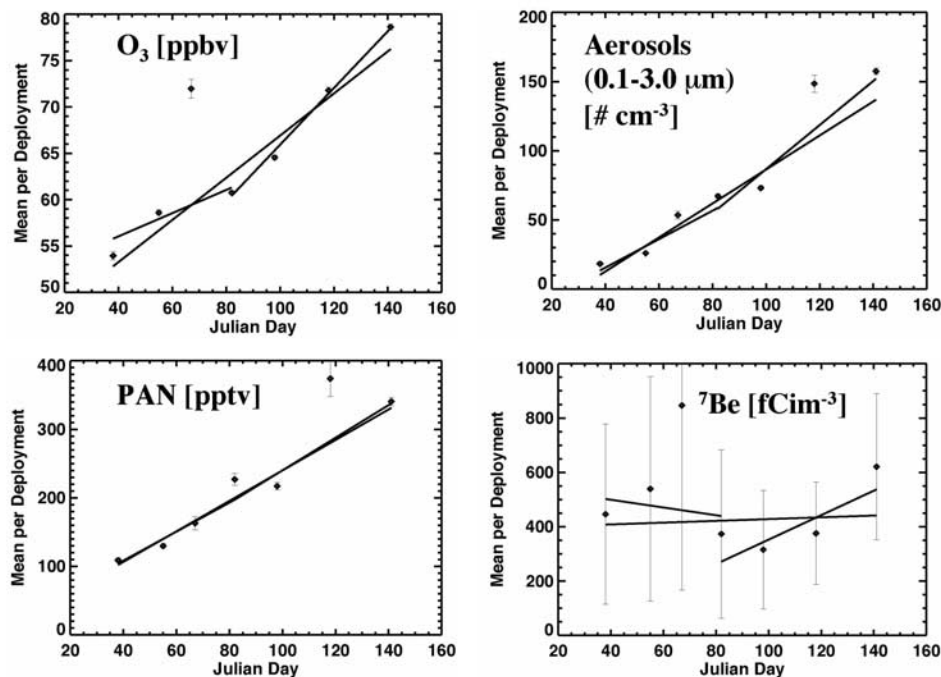

Figure 13. In situ measurement trends in mid troposphere ($4-6$ km) and high latitudes ($60°-85°N$). Vertical bars represent the standard error of the averages for O_3, aerosols, and PAN, and the standard deviation of the limited number of ^7Be measurements. Regression results are given in Table 4.

Table 4. In Situ Measurement Trends in $60°-85°N$, $4-6$ km Region During TOPSE

Parameter	Trend [chg/mo]	Trend [%/mo]	Initial Value (Day 38)	R
O_3[ppbv]	**6.82 ± 0.12**	**10.6**	**52.8**	**0.94**
CO [ppbv]	-1.11 ± 0.27	-0.78	144	-0.17
CH_4 [ppmv]	0.0041 ± 0.0003	0.22	1.815	0.48
H_2O [g/kg]	**0.027 ± 0.002**	**18.3**	**0.103**	**0.60**
N_2O [ppbv]	**5.64 ± 0.10**	**1.9**	**289**	**0.66**
NO [pptv]	**1.99 ± 0.09**	**23.3**	**5.23**	**0.67**
NO_2 [pptv]	-1.43 ± 0.16	-3.8	12.2	-0.10
NO_x [pptv]	1.56 ± 0.20	8.3	16.2	0.22
NO_y [pptv]	**53.0 ± 1.2**	**15.9**	**245**	**0.80**
PAN [pptv]	**66.8 ± 1.7**	**31.3**	**102.0**	**0.98**
SO_2 [pptv]	-1.24 ± 0.22	-8.9	15.9	-0.26
SO_4[pptv]	**56.1 ± 0.7**	**47.4**	**24.8**	**0.97**
J [NO_2] [$10^{-5} s^{-1}$]	**304 ± 3**	**33.8**	**392**	**0.99**
H_2SO_4 [10^3 cm^{-3}]	-14.2 ± 1.8	-10.3	161	-0.30
H_2O_2[pptv]	**42.1 ± 1.7**	**32.5**	**59.3**	**0.84**
CH_2O [ppbv]	**-0.019 ± 0.001**	**-16.6**	**0.143**	**-0.92**
Ethane [pptv]	**-98.0 ± 3.8**	**-6.3**	**1727**	**-0.75**
Ethyne [pptv]	**-79.5 ± 1.4**	**-20.0**	**529**	**-0.93**
Propane [pptv]	**-146.2 ± 2.2**	**-32.8**	**688**	**-0.97**
HCFC-141b [pptv]	**0.303 ± 0.010**	**2.2**	**13.3**	**0.96**
^7Be [fCi m^{-3}]	9.8 ± 102	2.3	407	0.08
Aero. (0.1–3 μm) [cm^{-3}]	**36.8 ± 0.6**	**51.4**	**10.3**	**0.96**

ratio of $O_3/^7Be$ for lower stratospheric air compares very well with a value of 0.060 ppbv/fCi m^{-3} found in stratospheric air in the Southern Hemisphere [*Browell et al.*, 2001]. The tropospheric background level of ^7Be in early February of 407 fCi m^{-3}, which would be a stratospheric equivalent of about 24 ppbv, is consistent with the PV analysis presented here, where we find that a significant component of background tropospheric O_3 was related to a relatively constant stratospheric source over the winter-spring transition, but the seasonal tropospheric O_3 increase was due predominantly to in-situ photochemical production. *Dibb et al.* [2003] also arrived at the same conclusion based on their analysis of the O_3 and ^7Be measurements during TOPSE.

[34] Table 4 presents a trend analysis for a selection of the trace gas, radiation, and aerosol data collected in the $60°-85°N$, $4-6$ km region during TOPSE. These data were limited to cases where the in situ O_3 was less than 100 ppbv to avoid including measurements above the tropopause in the averages. The trends in these parameters are given in absolute units/mo and as a percentage/mo based on the average TOPSE value from the linear regression line. The correlation coefficients are also given for the linear regression fit. Many of the parameters that are associated with continental pollution, surface source, or sunlight showed a high correlation with time during TOPSE ($|R| > 0.6$ for $>$ 85% confidence level for 7 points), and they are shown in bold in Table 4. The parameters with high positive correlation with time included: O_3, H_2O, N_2O, NO, NO_y, PAN, SO_4, J[NO_2], H_2O_2, HCFC-141b, and aerosols. The increase in H_2O and N_2O is significant since their main source is at the surface in the troposphere, and the increase in PAN in the free troposphere also cannot be a result of downward transport of stratospheric air (Flocke et al., submitted manuscript, 2002). In addition, fine aerosols (SO_4) showed a trend of increasing concentrations at increasingly higher altitudes during the TOPSE campaign (E. Scheuer et al., Seasonal distributions of fine aerosol sulfate in the North American Arctic Basin during TOPSE, submitted to *Journal of Geo-*

physical Research, 2002, hereinafter referred to as Scheuer et al., submitted manuscript, 2002). The hydrocarbons, including ethane, ethyne, and propane, showed a strong negative correlation with time due to increased photochemical consumption, and CH_2O also showed a net decrease over the period [*Fried et al.*, 2002]. The remainder of the parameters did not exhibit a statistically significant temporal correlation during TOPSE ($|R| < 0.5$), and they included: CO, CH_4, NO_x, SO_2, H_2SO_4, and, as discussed previously, ^7Be. Among the in situ parameters that were measured on the C-130, there were no trends that indicated a change in the level of stratosphere-troposphere exchange during TOPSE, but they strongly reflected continental pollution with active springtime photochemistry.

[35] The PAN results are in agreement with previous results with the qualification that the peak observed in Norway at Zeppelin Mountain ($77°55'N$, $11°54'E$) occurred in late April in 1994 [*Solberg et al.*, 1997a], and the trends in NMHCs are in agreement with previous results over the Baltic Sea and Finland [*Laurila and Hakola*, 1996] and Norway [*Solberg et al.*, 1997a].

[36] The decrease in SO_2 agrees with observations at Canadian stations from $42.9°$ to $51.7°N$ [*Dastoor and Pudykiewicz*, 1996; *Christensen*, 1997]. The increase in sulfate in the Arctic agrees with earlier work at Alert [*Cheng et al.*, 1993; *Dastoor and Pudykiewicz*, 1996], where it peaks around March or April. The same period for the peak was found during TOPSE (Scheuer et al., submitted manuscript, 2002). The observed increase in HCFC-141b reflects its general tropospheric trend because of increasing anthropogenic emissions [*Simmonds et al.*, 1998], and the increase in aerosols during the season is in agreement with measurements made at Alert by *Cheng et al.* [1993].

4. Summary and Conclusions

[37] The combination of the UV DIAL and in situ O_3 measurements made from the C-130 over the seven deployments of TOPSE conducted between 4 February and 23 May 2000 showed an average increase in O_3 at all altitudes across the free troposphere in the latitude range of $40°-85°N$. The largest average O_3 increases were found in the $40°-60°N$ region with 3.2 ppbv/mo in the $2-4$ km region and 6.1 ppbv/mo in the $4-6$ km region. At higher latitudes ($60°-85°N$), the average O_3 increase ranged from 3.0 ppbv/mo to 4.6 ppbv/mo in the $2-4$ km and $4-6$ km regions, respectively. A higher rate of O_3 increase was observed over the last four deployments of TOPSE in the higher latitudes with 5.0 ppbv/mo and 6.7 ppbv/mo in the $2-4$ km and $4-6$ km regions, respectively.

[38] Aerosol scattering ratios showed a dramatic increase across the free troposphere in all latitudinal regions investigated during TOPSE. In the $60°-85°N$, $4-6$ km region, S_A increased over 400% during TOPSE at an average rate of 0.36/mo. The average O_3 and aerosol scattering ratio levels were highly positively correlated over the TOPSE experiment with a correlation coefficient of 0.95 and an O_3/S_A slope of 10.6 ppbv. As has been observed in previous field experiments, if the source of additional O_3 was predominantly from the stratosphere, the correlation between O_3 and aerosol scattering would be negative since at the time of TOPSE the stratospheric air had low aerosol loading com-

pared to normal tropospheric conditions. This was the first indication that the predominant reason for the springtime O_3 increase at high latitudes was due to photochemistry and not stratosphere-troposphere exchange.

[39] The variation in PV during TOPSE was examined across the same regions as for O_3 and aerosol scattering, and the results from three models (MRF, HANK, and MOZART) were evaluated for an indication of any general trend in stratosphere-troposphere exchange that occurred during TOPSE. No statistically significant positive trend in PV was found for any of the model results in the entire $40°-85°N$, $2-6$ km region, and in general the average trend in PV over the field experiment was slightly negative. For example in the $60°-85°N$, $4-6$ km region, the trends ranged from 0.0054 PVU/mo from the MRF model to -0.0400 PVU/mo from the HANK model (MOZART gave -0.0353 PVU/mo). These results indicated that instead of there being an increased impact in this high-latitude region from stratosphere-troposphere exchange during TOPSE, there may have actually been a slight decrease in exchange.

[40] Since there is a change in the O_3/PV relationship in the lower stratosphere during the springtime, the impact of this change on the PV trend had to be evaluated. Using the monthly averages for O_3/PV in the lower stratosphere, it was determined that the stratospherically-derived O_3 trend was either zero or negative according to the HANK and MOZART models and only very slightly positive (0.39 ppbv/mo) for the MRF model. The results were the same using the Resolute O_3/PV data with the MRF model being the only model predicting a positive trend. It should be noted that regardless of the source of the O_3/PV ratio, all the models showed a strong negative trend during the period of the last three deployments, which was at a time that the overall O_3 positive trend was consistently the largest.

[41] The O_3 trend predicted by the MOZART chemical transport model was similar to that which was observed during the last half of TOPSE, and while the background level of O_3 can be mainly attributed to a stratospheric source, the O_3 change during TOPSE in the high-latitude troposphere was predominantly due to photochemistry. Backward trajectory analyses were conducted to investigate the source of air sampled during TOPSE, and these backward trajectories indicated that the air came from US/Canada and Eurasia with an increasing frequency during the field experiment. Most of the air exhibited some rising motion during the long-range transport to the Arctic, and very few air masses exhibited the descending motion that would be required with stratospheric air to contribute significantly to the tropospheric O_3 trend in this region. The ^7Be data show only a slight positive trend over the campaign, which amounts to less than 12% of the observed O_3 trend. In addition to the PV results, there were no trends in the in situ measurements that indicated a change in the level of stratosphere-troposphere exchange during TOPSE, but there were highly correlated trends in many gases and aerosols that strongly reflected active springtime photochemistry.

[42] Based on the above analysis, which examined: the O_3-S_A correlation; the estimate of stratospherically-derived O_3 trends from PV analyses and from the ^7Be data; and the in situ trace gas and aerosol trends, we estimate that stratosphere-troposphere exchange contributed less than 20% to the observed O_3 trend in the mid troposphere of the $60°-$ $85°N$ region across the spring equinox. The dominant source of the free tropospheric O_3 trend (>80%) was found to be photochemical O_3 production. This result validates the initial suggestion by *Penkett and Brice* [1986] and is in agreement with the recent findings of *Salisbury et al.* [2002] that the springtime O_3 maximum at high latitudes is largely a tropospheric phenomenon.

References

Appenzeller, E., J. R. Holton, and K. Rosenlof, Seasonal variation of mass transport across the tropopause, *J. Geophys. Res.*, *101*, 15,701–15,708, 1996.

Atlas, E., B. Ridley, and C. Cantrell, The Tropospheric Ozone Production about the Spring Equinox (TOPSE) Experiment: Introduction, *J. Geophys. Res*, doi:10.1029/2002JD003172, in press, 2003.

Brasseur, G. P., D. A. Hauglustaine, S. Walters, P. J. Rasch, J.-F. Muller, C. Granier, and X. X. Tie, MOZART: A global chemical transport model for ozone and related chemical tracers, 1, Model description, *J. Geophys. Res.*, *103*, 28,265–28,289, 1998.

Bridgman, H. A., R. C. Schnell, J. D. Kahl, G. A. Herbert, and E. Joranger, A major haze event near Point Barrow, Alaska: Analysis of probable source regions and transport pathways, *Atmos. Environ.*, *23*, 2537–2549, 1989.

Browell, E. V., Differential absorption lidar sensing of ozone, *Proc. IEEE*, *77*, 419–432, 1989.

Browell, E. V., A. F. Carter, S. T. Shipley, R. J. Allen, C. F. Butler, M. N. Mayo, J. H. Siviter Jr., and W. M. Hall, NASA multipurpose airborne DIAL system and measurements of ozone and aerosol profiles, *Appl. Opt.*, *22*, 522–534, 1983.

Browell, E. V., S. Ismail, and W. B. Grant, Differential absorption lidar (DIAL) measurements from air and space, *Appl. Phys. B*, *67*, 399–410, 1998.

Browell, E. V., E. F. Danielsen, S. Ismail, G. L. Gregory, and S. M. Beck, Tropopause fold structure determined from airborne lidar and in situ measurements, *J. Geophys. Res.*, *92*, 2112–2120, 1987.

Browell, E. V., C. F. Butler, S. A. Kooi, M. A. Fenn, R. C. Harriss, and G. L. Gregory, Large-scale variability of ozone and aerosols in the summertime Arctic and Sub-Arctic troposphere, *J. Geophys. Res.*, *97*, 16,433–16,450, 1992.

Browell, E. V., et al., Large-scale air mass characteristics observed over the Western Pacific during summertime, *J. Geophys. Res.*, *101*, 1691–1712, 1996a.

Browell, E. V., et al., Ozone and aerosol distributions and air mass characteristics over the South Atlantic Basin during the burning season, *J. Geophys. Res.*, *101*, 24,043–24,068, 1996b.

Browell, E. V., et al., Large-scale air mass characteristics observed over the remote tropical Pacific Ocean during March–April 1999: Results from PEM Tropics B Field Experiment, *J. Geophys. Res.*, *106*, 32,481–32,501, 2001.

Caplan, P., and H.-L. Pan, Changes to the 1999 NCEP operational MRF analysis/forecast system, *NWS Tech. Proc. Bull. 452*, Natl. Oceanic and Atmos. Admin., Washington, D. C., 2000.

Cheng, M.-D., P. K. Hopke, L. Barrie, A. Rippe, M. Olson, and S. Landsberger, Qualitative determination of source regions of aerosol in Canadian high Arctic, *Environ. Sci. Technol.*, *27*, 2063–2071, 1993.

Christensen, J. H., The Danish Eulerian hemispheric model: A three-dimensional air pollution model used for the Arctic, *Atmos. Environ.*, *24*, 4169–4191, 1997.

Dastoor, A. P., and J. Pudykiewicz, A numerical global meteorological sulfur transport model and its application to Arctic air pollution, *Atmos. Environ.*, *30*, 1501–1522, 1996.

Dibb, J., et al., Stratospheric influence on the North American free troposphere during TOPSE: ^{7}Be as a stratospheric tracer, *J. Geophys. Res*, doi:10.1029/2001JD001347, in press, 2003.

Djupstrom, M., J. M. Pacyna, W. Maehnaut, J. W. Winchester, S.-M. Li, and G. E. Shaw, Contamination of Arctic air at three sites during a haze event in late winter 1986, *Atmos. Environ. Part A*, *27A*, 2999–3010, 1993.

European Centre for Medium-Range Weather Forecasts (ECMWF), The description of the ECMWF/WCRP Level III-A global atmospheric data archive, Reading, U. K., 1995.

Emmons, L., et al., The budget of tropospheric ozone during TOPSE, *J. Geophys. Res*, doi:10.1029/2002JD002665, in press, 2003.

Fenn, M. A., et al., Ozone and aerosol distributions and air mass characteristics over the south Pacific during the burning season, *J. Geophys. Res.*, *104*, 16,197–16,212, 1999.

Grell, G. A., J. Dudhia, and D. R. Stauffer, A description of the fifth generation Penn State/NCAR Mesoscale Model (MM5), *NCAR/TN-398+IA*, 116 pp., Natl. Cent. for Atmos. Res., Boulder, Colo., 1993.

Hauglustaine, D. A., G. P. Brasseur, S. Walters, P. J. Rasch, J.-F. Muller, L. K. Emmons, and M. A. Carroll, MOZART: A global chemical transport model for ozone and related chemical tracers, 2, Model results and evaluation, *J. Geophys. Res.*, *103*, 28,291–28,355, 1998.

Hess, P. G., S. Flocke, J.-F. Lamarque, M. C. Barth, and S. Madronich, Episodic modeling of the chemical structure of the troposphere as revealed during the spring MLOPEX 2 intensive, *J. Geophys. Res.*, *105*, 26,809–26,839, 2000.

Holton, J. R., P. H. Haynes, M. E. McIntyre, A. R. Douglass, R. B. Rood, and L. Pfister, Stratosphere-troposphere exchange, *Rev. Geophys*, *33*, 403–439, 1995.

Iredell, M., and P. Caplan, Four-times-daily runs of the AVN model, *NWS Tech. Proc. Bull. 442*, Natl. Oceanic and Atmos. Admin., 3 pp., Washington, D. C., 1997.

Jursa, A. S., *Handbook of Geophysics and the Space Environment*, Air Force Geophys. Lab., Bedford, Mass, 1985.

Kanamitsu, M., Description of the NMC global data assimilation and forecast system, *Wea. Forecasting*, *4*, 335–345, 1989.

Kanamitsu, M., J. C. Alpert, K. A. Campana, P. M. Caplan, D. G. Deaven, M. Iredell, B. Katz, H.-L. Pan, J. Sela, and G. H. White, Recent changes implemented into the global forecast system at NMC, *Wea. Forecasting*, *6*, 425–435, 1991.

Klonecki, A., P. Hess, L. Emmons, L. K. Smith, J. Orlando, and T. S. Blake, Seasonal changes in the transport of pollutants into the Arctic- model study, *J. Geophys. Res*, doi:10.1029/2002JD002199, in press, 2003.

Laurila, T., and H. Hakola, Seasonal cycles of C_2-C_5 hydrocarbons over the Baltic Sea and Northern Finland, *Atmos. Environ.*, *30*, 1597–1607, 1996.

Monks, P. A., A review of the observations and origins of the spring ozone maximum, *Atmos. Environ.*, *34*, 3545–3561, 2000.

Pacyna, J. M., and M. Oehme, Long-range transport of some organic compounds to the Norwegian Arctic, *Atmos. Environ.*, *22*, 243–257, 1988.

Penkett, S. A., and K. A. Brice, The spring maximum in photo-oxidants in the Northern Hemisphere troposphere, *Nature*, *319*, 655–657, 1986.

Ridley, B. A., et al., Ozone depletion events observed in the high latitude surface layer during the TOPSE aircraft program, *J. Geophys. Res*, *108*(D4), 8356, doi:10.1029/2001JD001507, 2003.

Rummukainen, M., T. Laurila, and R. Kivi, Yearly cycle of lower tropospheric ozone at the Arctic circle, *Atmos. Environ.*, *30*, 1875–1885, 1996.

Salisbury, G., P. S. Monks, S. Bauguitte, B. J. Bandy, and S. A. Penkett, A seasonal comparison of the ozone photochemistry in clean and polluted air masses at Mace Head, Ireland, *J. Atmos. Chem.*, *41*, 163–187, 2002.

Schoeberl, M. R., et al., An assessment of the ozone loss during the 1999–2000 SOLVE/THESEO 2000 Arctic campaign, *J. Geophys. Res.*, *107*(D20), 8261, doi:10.1029/2001JD000412, 2002.

Seo, K.-H., and K. P. Bowman, A climatology of isentropic cross-tropopause exchange, *J. Geophys. Res.*, *106*, 28,159–28,172, 2001.

Simmonds, P. G., S. O'Doherty, J. Huang, R. Prinn, R. G. Derwent, D. Ryall, G. Nickless, and D. Cunnold, Calculated trends and the atmospheric abundance of 1,1,1,2-tetrafluoroethane, 1,1-dichloro-1-fluoroethane, and 1-chloro-1,1-difluoroethane using automated in-situ gas chromatography-mass spectrometry measurements recorded at Mace Head, Ireland, from October 1994 to March 1997, *J. Geophys. Res.*, *103*, 16,029–16,037, 1998.

Solberg, S., T. Krognes, F. Stordal, O. Hov, H. J. Beine, D. A. Jaffe, K. C. Clemitshaw, and S. A. Penkett, Reactive nitrogen compounds at Spitsbergen in the Norwegian Arctic, *J. Atmos. Chem.*, *28*, 209–225, 1997a.

Solberg, S., F. Stordal, and O. Hov, Tropospheric ozone at high latitudes in clean and polluted air masses, a climatological study, *J. Atmos. Chem.*, *28*, 111–123, 1997b.

Tie, X., et al., Effect of sulfate aerosol on tropospheric NOx and ozone budgets: Model simulations and TOPSE evidence, *J. Geophys. Res*, doi:10.1029/2001JD001508, in press, 2003.

Wang, Y., D. J. Jacob, and J. A. Logan, Global simulation of tropospheric O_3-NO_x-hydrocarbon chemistry, 3, Origin of tropospheric ozone and effects of nonmethane hydrocarbons, *J. Geophys. Res.*, *103*, 10,757–10,767, 1998.

————————————

E. L. Atlas, C. A. Cantrell, M. T. Coffey, K. Emmons, F. Flocke, A. Fried, J. W. Hannigan, P. G. Hess, A. A. Klonecki, B. Lefer, B. A. Ridley, L. X. Tie, A. J. Weinheimer, and B. Wert, National Center for Atmospheric Research, 1850 Table Mesa Drive, Boulder, CO 80305, USA.

D. R. Blake, Department of Chemistry, University of California, Irvine, Irvine, CA 92697, USA.

L. A. Brasseur, V. G. Brackett, C. F. Butler, M. B. Clayton, M. A. Fenn, and D. B. Harper, Science Applications International Corporation, One Enterprise Parkway, Suite 250, Hampton, VA 23666, USA.

E. V. Browell, W. B. Grant, J. W. Hair, and R. J. DeYoung, Atmospheric Sciences, NASA Langley Research Center, MS-401A, Hampton, VA 23681, USA. (e.v.browell@larc.nasa.gov)

J. E. Dibb and R. W. Talbot, Institute for the Study of Earth, Oceans, and Space, University of New Hampshire, Durham, NH 03824, USA.

J. A. Snow, Graduate School of Oceanography, University of Rhode Island, Kingston, RI 02881, USA.

A. J. Wimmers, Department of Environmental Sciences, University of Virginia, Charlottesville, VA 22904, USA.